



Western Washington University
Western CEDAR

WWU Graduate School Collection

WWU Graduate and Undergraduate Scholarship

Spring 2022

Synthesis, Characterization, and Applications of Thiolated Silk Fibroin

Jeremy Martinez Talusig
Western Washington University, jeremytalusig@gmail.com

Follow this and additional works at: <https://cedar.wwu.edu/wwuet>

 Part of the [Chemistry Commons](#)

Recommended Citation

Talusig, Jeremy Martinez, "Synthesis, Characterization, and Applications of Thiolated Silk Fibroin" (2022). *WWU Graduate School Collection*. 1089.
<https://cedar.wwu.edu/wwuet/1089>

This Masters Thesis is brought to you for free and open access by the WWU Graduate and Undergraduate Scholarship at Western CEDAR. It has been accepted for inclusion in WWU Graduate School Collection by an authorized administrator of Western CEDAR. For more information, please contact westerncedar@wwu.edu.

Synthesis, Characterization, and Applications of Thiolated Silk Fibroin

By

Jeremy Martinez Talusig

Accepted in Partial Completion
of the Requirements for the Degree
Master of Science

ADVISORY COMMITTEE

Dr. Amanda Murphy, Chair

Dr. Mike Larsen

Dr. John Antos

GRADUATE SCHOOL

David L. Patrick, Dean

Master's Thesis

In presenting this thesis in partial fulfillment of the requirements for a master's degree at Western Washington University, I grant to Western Washington University the non-exclusive royalty-free right to archive, reproduce, distribute, and display the thesis in any and all forms, including electronic format, via any digital library mechanisms maintained by WWU.

I represent and warrant this is my original work, and does not infringe or violate any rights of others. I warrant that I have obtained written permissions from the owner of any third party copyrighted material included in these files.

I acknowledge that I retain ownership rights to the copyright of this work, including but not limited to the right to use all or part of this work in future works, such as articles or books.

Library users are granted permission for individual, research and non-commercial reproduction of this work for educational purposes only. Any further digital posting of this document requires specific permission from the author.

Any copying or publication of this thesis for commercial purposes, or for financial gain, is not allowed without my written permission.

Jeremy Martinez Talusig

May 20, 2022

Synthesis, Characterization, and Applications of Thiolated Silk Fibroin

A Thesis
Presented to
The Faculty of
Western Washington University

In Partial Fulfillment
Of the Requirements for the Degree
Master of Science

by
Jeremy Martinez Talusig

Spring 2022

Abstract

Thiolated polymers, or thiomers, have demonstrated advanced adhesion to biological surfaces such as mucus membranes due to their ability to form disulfide bonds to the cysteine-rich domains in mucin making them an attractive drug delivery system. Silk fibroin, a protein derived from the *Bombyx mori* silkworm, offers a biocompatible and biodegradable platform absent in other thioimer systems. However, due to the small percentage of native cysteine residues in silk, installation of additional thiols is essential to create an advanced thioimer adhesive. In this research, covalent attachment of non-native thiols to the tyrosine residues of silk fibroin is accomplished with a high degree of functionalization. The extent of thiol modification is characterized by ultraviolet-visible spectroscopy (UV-VIS), proton nuclear magnetic resonance spectroscopy (^1H NMR), and ^1H - ^{15}N heteronuclear multiple bond correlation (HMBC). The reactivity of the thiol handles are probed using fluorescence spectroscopy and the *in situ* gelling ability of the thiolated silk is investigated using infrared spectroscopy (IR) and rheological measurements.

Acknowledgements

I would like to thank my lab colleagues for their continual support of my research. Also, this research could not have been accomplished without the help of Hla Win-Piazza, Sam Danforth, Kyle Mikkelsen and their instrument expertise. And most notably, I would like to thank my advisor, Dr. Murphy, for the guidance she has given the past four years and inspiring me to be the scientist that I am today.

I would also like to thank my family and my partner for encouraging and supporting me through all my life endeavors. For that reason, all of my accomplishments are their accomplishments as well. Lastly, I would like to thank my dogs, for keeping me company during late nights of research and writing.

Table of Contents

Abstract.....	iv
Acknowledgements.....	v
List of Tables and Figures.....	viii
Chapter 1. Introduction	1
1.1 Silk Fibroin Characteristics and Applications	1
1.2 Chemical Modification of Silk Fibroin	2
1.3 Thiol Functionalization of Silk Fibroin.....	4
1.4 Thiolated Polymers for Mucoadhesive Drug Delivery Systems.....	5
Research Aims.....	9
Chapter 2. Materials and Methods.....	10
2.1 Instrumentation	10
2.2 Preparation of Aqueous Silk Solution	10
2.3 Diazonium Coupling on Silk Solution	11
2.4 Reduction of Acid-Modified Silk Solution	12
2.5 Sulfo-SPDP Modification of Amtyr-Silk.....	12
2.6 Reduction of SPDP-Silk.....	12
2.7 Fluorescent Attachment of SPDP-Silk.....	13

2.8 Gelation of Thiol-Silk.....	13
2.9 Rheometric Measurements of Silk Samples	13
Chapter 3. Results and Discussion	14
3.1 Amine Functionalization of Tyrosine	14
3.2 Sulfo-SPDP Modification of Amtyr-Silk	15
3.3 Reduction of SPDP-Silk.....	18
3.4 Conjugation of IAEDANS to Thiol-Silk	21
3.5 In Situ Gelation of Thiol-Silk.....	25
3.6 Rheological Investigation of Thiol-Silk	28
Chapter 4. Conclusions	31
References	33

List of Tables and Figures

Figure 1. Beta sheet composition of silk fibroin	2
Figure 2. Summary of thiol-functionalization performed on silk fibroin.....	5
Figure 3. Common thiomers studied for mucoadhesion.....	7
Figure 4. Proton NMR of amtyr-silk	15
Figure 5. Proton NMR of SPDP-silk	17
Figure 6. ^1H - ^{15}N HMBC of SPDP-silk	18
Figure 7. Proton NMR of thiol-silk with pyridine-2-thione.....	20
Figure 8. Proton NMR of purified thiol-silk.....	20
Figure 9. UV-VIS spectra of SPDP-silk and thiol-silk.....	21
Figure 10. Fluorescence spectrum of AEDAN-silk.....	23
Figure 11. Proton NMR of AEDAN-silk	24
Figure 12. ^1H - ^{15}N HMBC of AEDAN-silk.....	25
Figure 13. <i>In Situ</i> gelation of thiol-silk	26
Figure 14. FTIR spectra of thiol-silk gel, unmodified silk gel, and silk solution	27
Table 1. FTIR vibrational band assignments	28
Table 2. Apparent viscosity and modulus for varying concentrations of thiolated silk	29

Chapter 1. Introduction

1.1 Silk Fibroin Characteristics and Applications. The study of silk has gained traction in the past decades for its potential use in biomedical applications. The popularity of silk fibroin can be attributed to the fact that it is easily processable,¹ biocompatible, biodegradable,²⁻⁴ and has robust mechanical properties.⁵ The most commonly studied silk is produced by the *Bombyx mori* silkworm and contains 5,263 amino acids, the majority of which are glycine (45.9 mol%), alanine (30.3 mol%), and serine (12.1 mol%).⁶ The silk cocoons from the *Bombyx mori* can be re-processed into different structures including fibers,⁷ hydrogels,^{8,9} films,^{4,10} and solutions¹¹ giving silk the opportunity to be studied under a variety of experimental conditions.

The strong mechanical properties of silk fibroin can be attributed to its hierarchical structural organization. Silk fibroin consists of 12 hydrophobic crystalline domains each linked by hydrophilic amorphous regions. Within these crystalline domains are repeating amino acid units of glycine-alanine-glycine-alanine-glycine-serine (GAGAGS), which can self-assemble and stack into anti-parallel beta sheets due to hydrogen bonding and van der Waals forces (Figure 1). The mechanical properties of solid silk structures can be further tuned by controlling the degree of self-assembly within the crystalline regions, making silk versatile for various applications such as tissue engineering,^{12,13} implantable devices, textiles, and cosmetics.¹⁴

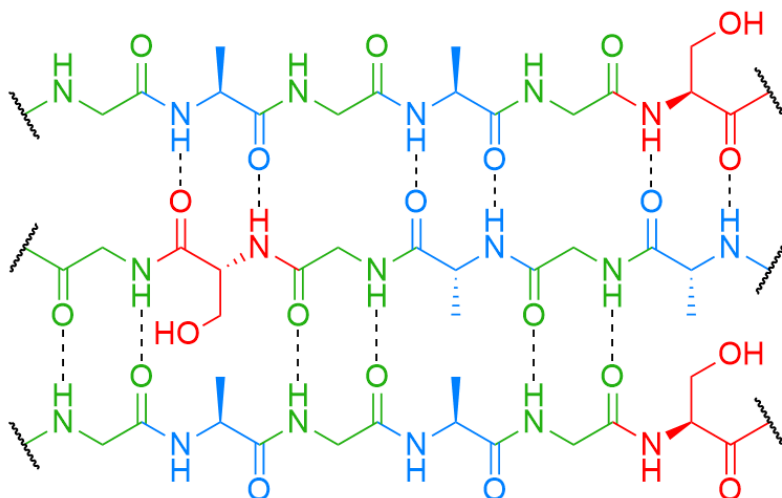


Figure 1. Hydrogen bonding between repeating units of GAGAGS that form the crystalline antiparallel beta sheets of silk fibroin.

The less abundant amino acids that make up silk fibroin can be found mainly in the amorphous regions of the protein. Tyrosine residues are present at 5.3 mol%, and exist in both the crystalline and amorphous regions, while 16 other amino acids are present at a total of 6.6 mol% of silk and are only located in the amorphous regions.⁶ Because the majority of amino acids in silk are inert, the popular amino acids for chemical modification such as lysine, aspartic acid, and glutamic acid are present in extremely low amounts.

1.2 Chemical Modification of Silk Fibroin. In recent decades, researchers have investigated methods to chemically modify the reactive sites of silk fibroin (in solid structure and aqueous form) for medical applications such as of drug delivery, cell proliferation, muscle regeneration and more.^{15,16} As previously mentioned, a majority of silk is composed of the inert amino acids glycine and alanine (76.2 mol% combined). However, a small fraction of the amino acids in silk are reactive and available for modification including serine (12.1 mol%), threonine (0.9 mol%),

tyrosine (5.3 mol%), aspartic acid (0.5 mol%), and glutamic acid (0.6 mol%). Modification of serine is typically avoided as it is integral to the crystalline beta sheet structure of the protein.

Isocyanate coupling,¹⁷ carbodiimide coupling,¹⁸ and diazonium coupling¹⁹ are just a few methods that have been utilized to create covalent linkages to native functional groups within silk fibroin. Isocyanate coupling targets the serine, threonine, and lysine residues of silk to create urea or urethane linkages. While isocyanate coupling has been reported on silk films, degummed fibers, and fabric, the reaction generally requires the use of organic solvent, which should be avoided as much as possible when working with any protein.^{17,20} Another common coupling agent used to crosslink proteins is 1-ethyl-3-(3-dimethylaminopropyl)carbodiimide (EDC), which works through the production of an amide bond from the reaction between a carboxyl group and a primary amine. The EDC reaction involves several side reactions that can compete with amide formation producing undesired products such as an inactive isourea product, an inactive N-acylisourea derivative, and anhydride formation.²¹ Because many proteins and small biomolecules contain both a carboxyl and an amine functional group, variability in products is possible including undesired crosslinked biomolecules and inter- and intramolecular crosslinks within silk itself (SF-SF), which consequently may alter the physical properties of silk. Diazonium coupling is another popular and powerful covalent modification performed on silk and incorporates aniline derivatives on the tyrosine residues of silk through azo bonds. The azo bonds produce a color change to the silk from colorless to dark red due to the increased conjugation system—a characteristic that may interfere with optical assays. While this is a well utilized and rapid reaction, the acidity of the diazonium coupling may prevent this chemistry from being performed in more complex, biological settings.

1.3 Thiol Functionalization of Silk Fibroin. Of the extensive list of chemical modifications that can be performed on silk, chemistry involving thiols has not been as widely explored. Thiols are important bridging structures in nature as proven by their existence in polysaccharides, proteins, and natural products. Their relatively low pKa allows them to be highly reactive in physiological conditions²² and their ability to form cleavable disulfide bonds make them a popular site for protein labeling and crosslinking.^{23,24}

Customary protein modification is accomplished on the nucleophilic sites of the protein, such as the lysine or cysteine residues. However, cysteines, the only thiol-bearing amino acid, are present in extremely low concentrations in silk fibroin—making up less than 0.1 mol% of the amino acid content in silk.⁶ As a consequence, chemical modifications targeting the native cysteine sites on silk ultimately result in low levels of modification. Therefore, incorporation of non-native sulfhydryl groups to the more abundant reactive sites of silk presents the opportunity to selectively attach functionalized molecules via thiol chemistry that was limited before. The Dahr and Zhang group have both reported the incorporation of thiol containing molecules (cysteine and glutathione, respectively) onto the aspartic and glutamic acid residues of silk by EDC-NHS coupling, as seen in Figure 2A-B.^{25,26} Still, aspartic and glutamic acid merely make up a combined 1.5 mol% of silk, therefore the extent of modification by carbodiimide coupling is limiting. Laomopheel et al. outlined another procedure to functionalize silk with sulfhydryl groups by targeting the lysine residues of silk (0.2 mol%) with 2-iminothiolane (Traut's reagent) for the formation of hydrogels (Figure 2D).²⁷ With the same goal to create crosslinked hydrogels, the Ki group also functionalized the lysine residues of silk with dithiothreitol (DTT) by the attachment of norbornene molecules followed by thiol-ene click chemistry (Figure 2C).²⁸ Although thiol

containing molecules were successfully incorporated onto the lysine residues of silk for chemical crosslinking, using these residues as functional targets only result in 0.2 mol% of modification—the same limitation posed by carbodiimide coupling. Additionally, the studies fail to demonstrate the ability for the thiol bearing molecules to be cleaved for the attachment of other functionalized molecules via disulfide bonds. The lack of methods for the installation of cleavable thiols into silk at unconventional amino acid sites with a high degree of functionalization warrants further research.

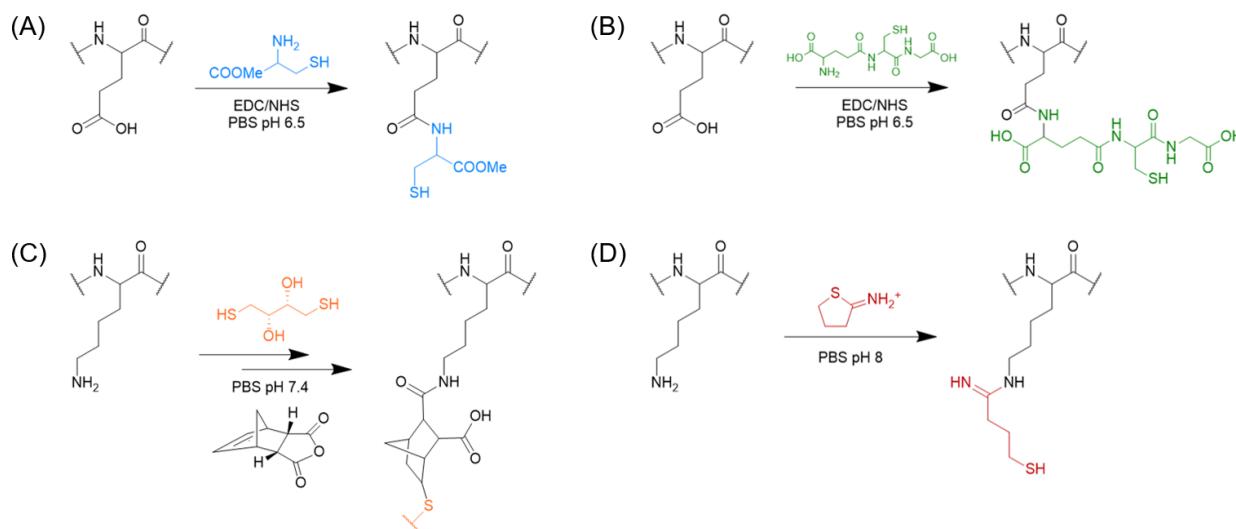


Figure 2. Summary of thiol-functionalization performed on silk fibroin. (A-B) Attachment of cysteine and glutathione to the aspartic and glutamic acid residues of silk fibroin using carbodiimide coupling.^{25,26} (C) Attachment of norbornene molecules to the lysine residues of silk followed by thiol-ene click chemistry.²⁸ (D) Attachment of 2-iminothiolane to the lysine residues of silk.²⁷

1.4 Thiolated Polymers for Mucoadhesive Drug Delivery Systems. Mucus membranes are important barriers that line and protect important systems and organs within the body such as the gastrointestinal tract, respiratory tract, eyes, nose, and other cavities within the body. Mucus, secreted by epithelial cells lining organs, is generally made up of 95% water, inorganic salts, lipids

and mucin glycoproteins, a mixture responsible for the viscous gel consistency of these membranes.²⁹ Depending on the mucosal surface within the body, the mucus layer will vary in thickness and composition.²⁹ Despite slight variation, all mucus membranes serve as a protective barrier for epithelial cells from pathogens in the lumen while regulating the absorption and passage of important nutrients and small molecules.³⁰

Intimate contact between a mucosal surface and a substrate is a phenomenon known as mucoadhesion and is the consequence of a combination of hydrophobic, van der Waals, electrostatic, and chemical interactions.²⁹ This interfacial interaction has been studied as a system for drug delivery due to its merit of prolonged residence time, an attractive trait for drug absorption. The first generation of mucoadhesives studied for drug delivery include polymers containing numerous hydrogen-bonding groups capable of forming a strong non-specific attraction to mucus membranes and other wet surfaces for site delivery. Examples of first generation polymers include chitosan,³¹ polyacrylic acid,³² and cellulose derivatives.³³ However, in recent decades, a second generation of mucoadhesives has emerged with increased site specificity and adhesive power. Polymers containing thiol groups have been shown to form disulfide bonds with the cysteine rich domains of mucin glycoproteins in mucus membranes.³⁴ Thiol-functionalized polymers have demonstrated an increase in residence time at the mucosal site, enhanced membrane permeation, and bioavailability.³⁵ Thiolated chitosan,^{36,37} thiolated polyacrylic acid,³⁸ thiolated polyallylamine³⁹ and thiolated cellulose derivatives⁴⁰ have all been explored for mucoadhesive properties (Figure 3), and have demonstrated improved adhesion compared to their unmodified analogues.

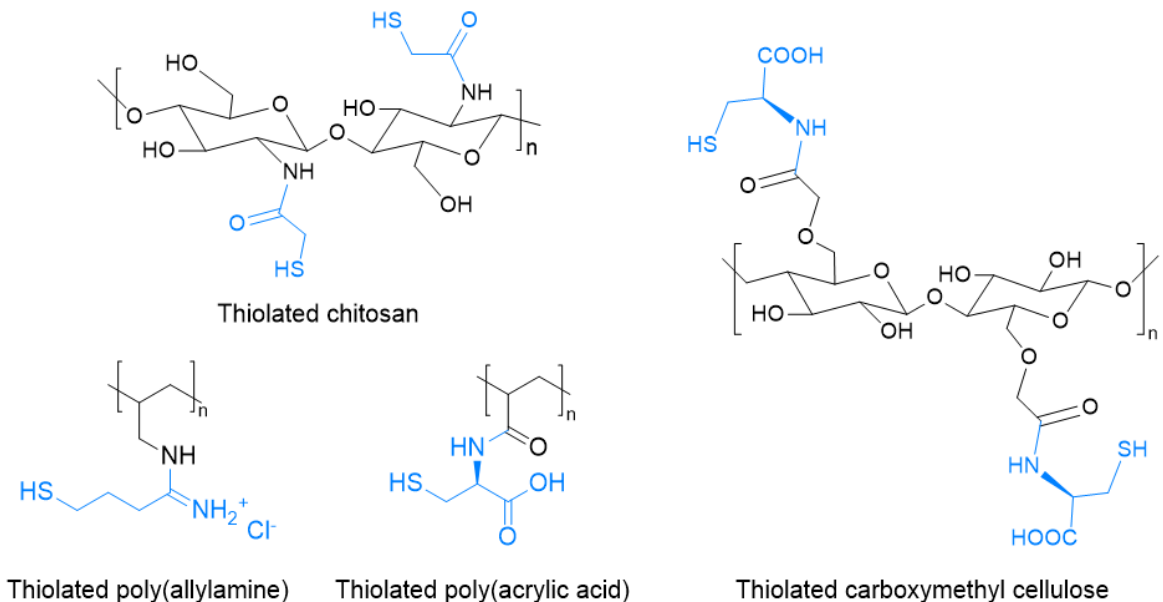


Figure 3. Common thiolated polymers studied for mucoadhesion. Thiol moieties added are highlighted in blue.

Another notable trait that thiolated polymers display is *in situ* gelling due to oxidative crosslinking. Rapid clearance at the site of drug administration can greatly reduce the adsorption of drugs and *in situ* gelling of polymer formulations has been a common approach to address the issue. Thiolated chitosan such as chitosan-thioglycolic acid derivatives have demonstrated solution-gel transitions resulting in more than a 10,000 fold increase in dynamic viscosity while in the presence of oxidizing agents and physiological pH.⁴¹ Further, disulfide exchange between thiolated polymers with the free thiol moieties in mucin have been observed to cause an increase in dynamic viscosity thus triggering *in situ* gelling at the site of contact without the need of an exogenous oxidizing source. The advanced adhesion and *in situ* gelling that thiolated polymers demonstrate are promising properties for advancements in mucoadhesive drug delivery systems.

While silk fibroin has been extensively studied as a vehicle for drug delivery, it has yet to be explored as a second generation mucoadhesive that is functionalized with free thiol moieties. The biodegradability, tunable mechanical properties, and ability to be chemically functionalized make silk fibroin a strong candidate as a natural polymer for mucoadhesives.

Research Aims

The first aim of this research was to chemically incorporate free thiols to the tyrosine residues of silk fibroin. Once incorporated, we sought to characterize the new thiol-modified silk (thiol-silk) using ^1H NMR, ^1H - ^{15}N HMBC, and UV-VIS.

The second aim of this research was to probe the reactivity of the newly installed sulfhydryl groups using a thiol-specific fluorescent molecule and fluorescence spectroscopy to support successful conjugation. The last aim was to determine if the thiol-silk could form inter- and intramolecular disulfide bonds for *in situ* gelling using rheometric measurements.

Chapter 2. Materials and Methods

2.1 Instrumentation. Proton nuclear magnetic resonance spectroscopy (^1H NMR) of silk solutions was performed on a Bruker Avance III 500 MHz spectrometer. Fourier transform infrared (FTIR) of silk gels were recorded on a Thermo Nicolet 6700 FTIR using an attenuated total reflectance (ATR) crystal. Ultraviolet-Visible spectroscopy (UV-Vis) of silk solutions were collected using a Jasco UV-VIS-NIR spectrometer and fluorescence spectra collected on a BioTek Synergy H1MF model plate reader. Lastly, a Discovery HR-2 rheometer by TA Instruments was used to collect viscosity measurements of the silk gels.

2.2 Preparation of Aqueous Silk Solution. In 1.5 L of 0.02 M Na_2CO_3 , 12 *Bombyx mori* silkworm cocoons were cut into 8 equal pieces and boiled for 1 h. The silk fibers were then removed from the boiling Na_2CO_3 and placed in 1.5 L of boiling DI water for 10 min. Remaining sericin was removed by rinsing the fibers in 2 L of room temperature DI water, repeating this rinse 3x. Once completely rinsed, the silk fibers were allowed to dry overnight.

The dry mass of the fibers were measured and then coated in 9.3 M LiBr to create a 20% (w/v) solution (5 mL LiBr per g of silk). The LiBr coated fibers were placed in a 60 °C oven for 1 h, or until all of the silk fibers completely dissolved in the LiBr. The dissolved silk was transferred to a hydrated dialysis tube (MWCO 3,500) and dialyzed against 3 L of DI water, changing the water after one hour, then after an additional three hours, and then left to dialyze overnight. The dialysis water was changed the next morning, afternoon, and evening. If the silk solution was too acidic or basic, 1 M NaOH or HCl was added to the dialysis water and dialysis of the silk continued until the silk solution remained neutral. The silk solution was concentrated by letting the dialysis

bag containing the silk solution sit in dry polyethylene glycol (PEG, MW 12k) for several hours until the concentration was approximately 2-4 wt%. The silk solution was then pipetted into a fritted syringe (Torviq #SF-5000) and dispensed to remove any leftover dust debris floating in the solution. The silk solution was stored in a refrigerator. Unmodified silk ^1H NMR (500 MHz, D_2O , δ): 7.4-7.2 (m, 1H), 7.1 (m, 2H), 6.8 (m, 2H), 4.6-4.4 (m, 3H), 4.3 (m, 6H), 4.0 (m, 21H), 3.1-2.9 (m, 2H), 1.5-1.2 (m, 17H), 1.0-0.8 (m, 3H)

2.3 Diazonium Coupling on Silk Solution. To prepare the silk solution for diazonium coupling, the silk was exchanged into 100 mM borate buffer (136 mM NaCl, pH 9.4) by dialysis. Once in borate buffer, 16.0 mL of the silk solution was allowed to cool on ice for at least 15 min. Meanwhile, a diazonium salt solution was prepared by dissolving 69.6 mg (0.4 mmol) of sulfanilic acid and 304 mg (1.6 mmol) of p-toluene sulfonic acid (pTSA) in 4 mL of nanopure water and the solution cooled on ice for 10 min. After cooling, 136 μL (0.5 mmol) of isotopically labeled 4 M sodium nitrite ($\text{Na}^{15}\text{NO}_2$, Cambridge Isotope Laboratories, Inc.) was pipetted into the sulfanilic acid/pTSA solution and cooled for an additional 15 min. The resulting diazonium salt solution was then poured into the 16.0 mL of cooled silk, inverted, and left to react on ice for 40 min. Once the reaction was completed, the acid-modified silk solution (azo-silk) dialyzed against DI water, changing the water 3x over the next 16 h, and then dialyzed against borate buffer for an additional 24 h. The diazonium coupling was repeated on the same azo silk to produce a doubly acid-modified silk solution to ensure all tyrosine residues were modified with sulfonic acid groups. Azo-silk ^1H NMR (500 MHz, D_2O , δ): 7.9 (m, 4H), 7.4-6.8 (m, 3H), 4.5 (m, 1H), 4.3 (m, 1H), 4.2 (m, 6H), 4.0-3.9 (m, 19H), 3.0-2.9 (m, 2H), 2.0 (1H), 1.4-1.3 (m, 16H), 0.8 (m, 3H)

2.4 Reduction of Acid-Modified Silk Solution. In 1.0 mL of ~4 wt% azo-silk, 95.2 mg (0.06 mmol, 18 equivalents relative to the number of tyrosine residues) sodium dithionite was dissolved, and the solution was left to react for 30 min at rt to produce amine-functionalized silk (amtyr-silk). The reaction solution was passed through a NAP-10 column (Cytiva) pre-equilibrated with PBS pH 7.2 for purification. For NMR, 0.5 mL of purified amtyr-silk was exchanged into D₂O using a NAP-5 column. Amtyr-silk ¹H NMR (500 MHz, D₂O, δ): 7.3 (m, 1H), 6.8-6.4 (m, 3H), 4.5 (m, 2H), 4.3 (m, 4H), 4.2-3.8 (m, 13H), 3.1-2.7 (m, 2H), 2.1 (m, 1H), 1.6-1.1 (m, 12H), 1.0-0.7 (m, 3H)

2.5 Sulfo-SPDP Modification of Amtyr-Silk. Immediately after the reduction and purification of amtyr-silk, 32.0 mg (0.06 mmol, 3 equivalents relative to the number of tyrosine residues) of sulfosuccinimidyl 6-(3'-(2-pyridyldithio)propionamido)hexanoate (sulfo-LC-SPDP, Campbell Science) was dissolved in 1.0 mL of ~3 wt% amtyr-silk, and allowed to react for 1 h at room temperature with rocking. The reaction solution was passed through a NAP-10 column pre-equilibrated with PBS pH 7.2 for purification. For NMR, 0.5 mL of purified SPDP-modified silk (SPDP-silk) was exchanged into D₂O. SPDP-silk ¹H NMR (500 MHz, D₂O, δ): 8.2 (m, 1H), 8.1-7.4 (m, 3H), 7.4-6.9 (m, 3H), 6.8 (m, 1H), 4.5 (m, 3H), 4.3 (m, 6H), 4.1-3.8 (m, 21H), 3.3-2.7 (m, 6H), 2.7-2.2 (m, 3H), 1.6-1.5 (m, 3H), 1.5-1.0 (m, 21H), 1.0-0.7 (m, 3H)

2.6 Reduction of SPDP-Silk. To 1.0 mL of ~2 wt% SPDP-silk, 11.6 mg (0.04 mmol, 3 equivalents relative to the number of tyrosine residues) of tris(2-carboxyethyl)phosphine hydrochloride (TCEP-HCl) was dissolved and left to react for 10-15 min. For purification, the reaction was centrifuged using a Vivaspin 6 (MWCO 10,000) for 45 min at 4000 RPM and 4 °C. For NMR, 0.5 mL of the purified reduced silk (thiol-silk) was exchanged into D₂O using a NAP-5 column. Thiol-

silk ^1H NMR (500 MHz, D_2O , δ): 8.0-7.5 (m, 1H), 7.3 (m, 1H), 6.9 (m, 1H), 4.5 (m, 2H), 4.3 (m, 5H), 4.0-3.8 (m, 19H), 3.1 (m, 2H), 3.0-2.6 (m, 2H), 2.5 (m, 2H), 1.8-1.5 (m, 2H), 1.5-1.1 (m, 21H), 1.0-0.7 (m, 3H)

2.7 Fluorescent Attachment of SPDP-Silk. To covalently attach the fluorescent molecule 5-((((2-iodoacetyl)amino)ethyl)amino)naphthalene-1-sulfonic acid), or IAEDANS, to the reduced thiolated silk, 28.6 g (0.06 mmol, 7.5 equivalence relative to the number of tyrosine residues) of IAEDANS was dissolved in 1 mL of ~ 1 wt% thiol-silk and left for 3 h at rt. To keep the reaction from degrading in light, the reaction was performed in the dark, covered in foil. Afterwards, the reaction solution was passed through a NAP-10 column pre-equilibrated with PBS pH 7.2 and if NMR was needed, exchanged into D_2O using a NAP-5 column. AEDAN-Silk ^1H NMR (500 MHz, D_2O , δ): 8.2-7.9 (m, 2H), 7.6-7.0 (m, 4H), 6.9 (m, 2H), 6.6 (m, 1H), 4.5 (m, 2H), 4.3 (m, 4H), 4.1-3.7 (m, 12H), 3.5 (m, 1H), 3.3-2.7 (m, 6H), 2.7-2.4 (m, 2H), 2.3 (m, 3H), 2.1 (m, 1H), 1.7-1.5 (m, 2H), 1.4-1.0 (m, 13H), 1.0-0.7 (m, 3H)

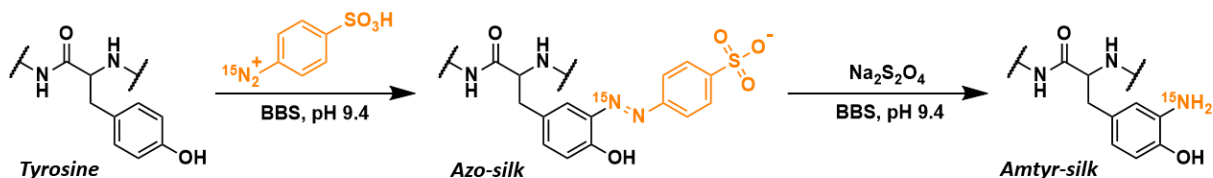
2.8 Gelation of Thiol-Silk. To acquire different concentrations of the reduced silk for gelation studies, the thiol-silk was diluted to concentrations of 2.5, 5, and 10 wt% using PBS pH 7.2 after being spin concentrated for the removal of TCEP-HCl. The thiol-silk was then allowed to sit at rt to observe gelation or any changes in viscosity over time.

2.9 Rheometric Measurements of Silk Samples. Rheometric measurements were performed on a TA Instruments Discovery HR-2 rheometer at rt. In a 15 mm parallel plate geometry, 0.5 mL of silk sample was loaded and subjected to a constant shear rate of 1 s^{-1} (no relaxation) and its apparent viscosity and shear modulus averaged over 3 min and recorded.

Chapter 3. Results and Discussion

3.1 Amine Functionalization of Tyrosine. Tyrosine residues of silk needed to be functionalized with nucleophilic amines prior to the attachment of disulfide containing molecules (Scheme 1). To do this, a diazonium coupling reaction was performed on the silk solution to install negatively charged sulfonic acid groups as previously reported by Murphy et al.¹⁹ The diazonium coupling produced a color change of the silk solution from colorless to dark red which was indicative of the formation of azo bonds and the attachment of a larger conjugated system to the tyrosine residues. Once sulfonic acid groups were installed, sodium dithionite was used to reduce the azo bonds to primary amines ortho to the hydroxyl group on tyrosine.

Scheme 1. Diazonium coupling of tyrosine residues to produce azo-silk and subsequent reduction to form amine functionalized tyrosine residues (amtyr-silk). Structures containing isotopically labeled nitrogen are indicated in orange.



Changes to the aromatic region in the proton NMR of plain silk demonstrate the functionalization of the tyrosine ring with a primary amine. Two peaks corresponding to the two types of protons on unmodified tyrosine can be seen at 6.7 and 7.0 ppm (Figure 4B). Once functionalized with an amine, the tyrosine ring now contains three unique types of protons whose resonances can be observed at 6.5, 6.6, and 6.7 ppm (Figure 4A).

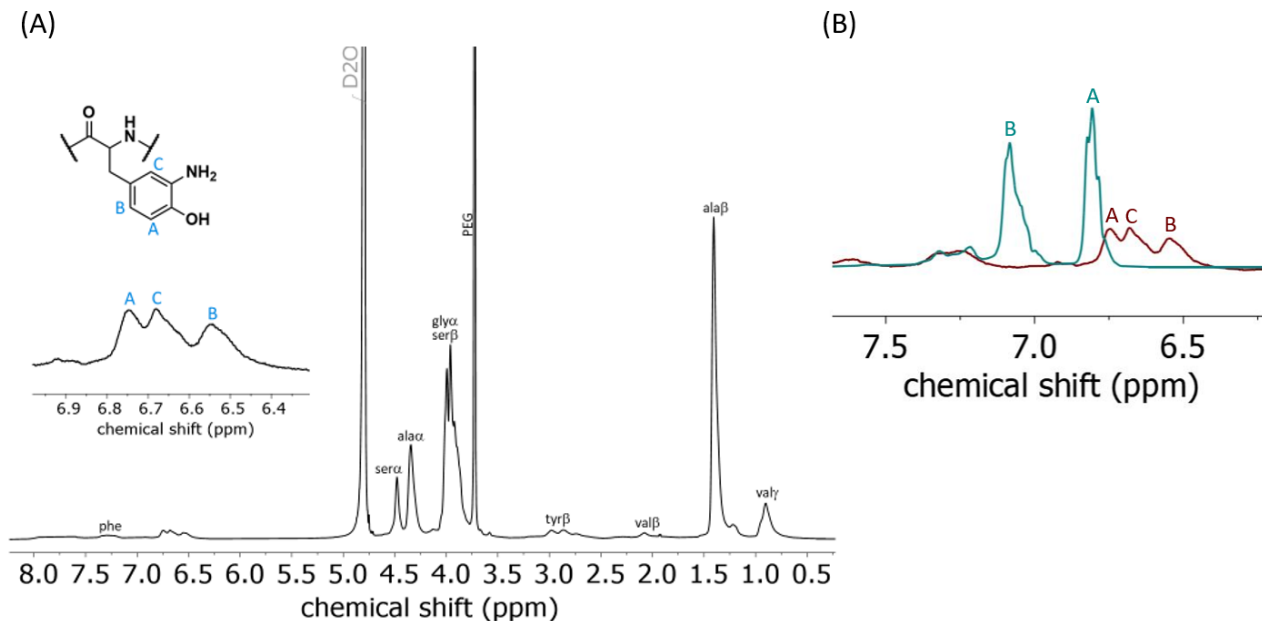
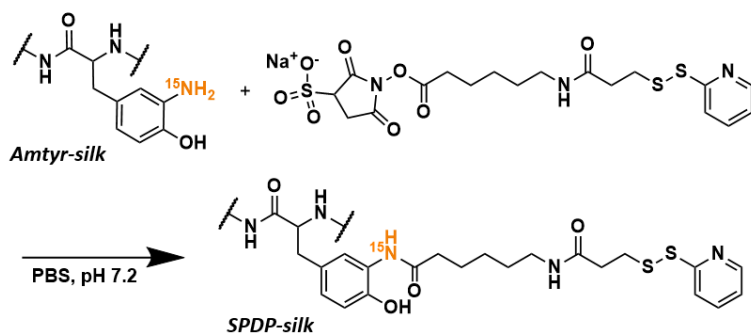


Figure 4. (A) ¹H NMR of aminotyrosine-silk with an expansion of the aromatic region. (B) Spectra overlay of the aromatic regions of unmodified silk (teal) and aminotyrosine-silk (burgundy).

3.2 Sulfo-SPDP Modification of Amtyr-Silk. To avoid degradation, it was necessary to use the amtyr-silk for reaction right away as the electron-rich tyrosine ring is prone to further oxidation. In early experiments, the heterobifunctional crosslinker succinimidyl 3-(2-pyridyldithio)propionate (SPDP) was used for disulfide attachment into silk. However, because SPDP is not water soluble and must be dissolved in dimethyl sulfoxide prior to reaction, solubility and purification became problematic with larger scale reactions. For this reason, sulfo-LC-SPDP was instead utilized due to its aqueous solubility and in turn was easier to purify. Accordingly, 3 equivalents of sulfo-LC-SPDP was dissolved in amtyr-silk immediately once purified (Scheme 2). During the 1 h reaction of sulfo-LC-SPDP modification, the reaction solution became cloudy within 15-30 min and by the end of the reaction, gelled silk was observed on the sides of the tube containing the SPDP-modified silk. It is hypothesized that because sulfo-LC-SPDP contains a

hydrophobic methylene chain, the nonpolar group installed was enough to cause some silk to gel. After purification using a size exclusion column, it was noted that SPDP-silk no longer displayed cloudiness, suggesting that the gelled silk was lost to the column.

Scheme 2. Modification of aminotyrosine-silk with sulfo-LC-SPDP to produce SPDP-silk.



The SPDP-silk was characterized using ^1H NMR, ^1H - ^{15}N -HMBC, and UV-VIS. Drastic changes were noticed in the aromatic and methylene region of the proton NMR of SPDP-silk (Figure 5A). Where there were once only three peaks in the aromatic region of amtyr-silk, five new peaks appear at different chemical shifts (Figure 5B). A tall single peak at 8.2 ppm can be attributed to the characteristic pyridine proton from the attached sulfo-LC-SPDP molecule. The remaining pyridine protons, K/L and M were assigned to peaks at 7.5 and 7.0 ppm, respectively, using Mnova predictions and confirmed with HMBC. The chemical shifts of tyrosine protons A and B are so close in resonance they are assigned to one broad peak at 6.8 ppm, and tyrosine proton C can be seen slightly more downfield at 7.3 ppm. The electron-withdrawing amide group pulling electron density away from the aromatic ring is thought to be responsible for the increasing chemical shifts of protons A, B, and C of from amtyr-silk to SPDP-silk.

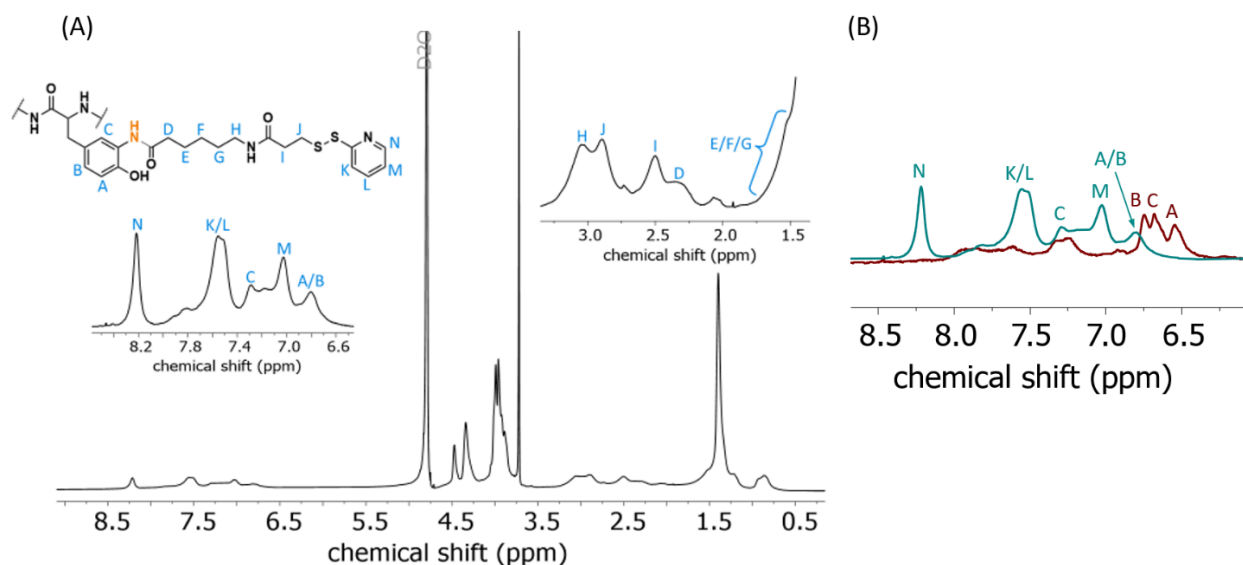


Figure 5. (A) ¹H NMR of sulfo-SPDP modified silk with expansions of the aromatic and methylene regions. (B) Spectra overlay of the aromatic regions of amtyr-silk (burgundy) and SPDP-silk (teal).

Changes to the methylene region of the amtyr-silk spectrum further corroborate the attachment of sulfo-LC-SPDP. In the 2.5-3.5 ppm region of the amtyr-silk NMR, the only methylene peaks seen are those that belong to the beta protons of tyrosine (Figure 4). Once sulfo-LC-SPDP is covalently attached, four new peaks arise coming from the methylene protons of sulfo-LC-SPDP.

Another characterization method that was employed was the use of heteronuclear multiple bond correlation (HMBC) between the isotopically labeled nitrogen and adjacent hydrogens. During the diazonium coupling reaction, ¹⁵N was used in the diazonium salt solution for the installation of isotopically labeled nitrogen to confirm and characterize amide bond formation. In Figure 6, a cross peak at (7.27, 127.77) ppm can be seen corresponding to the coupling between aromatic proton C and the installed ¹⁵N. Although HMBC coupling can occur over 3-4 bonds, interestingly, a cross peak was not observed between the ¹⁵N and the adjacent methylene protons on the other side of the amide.

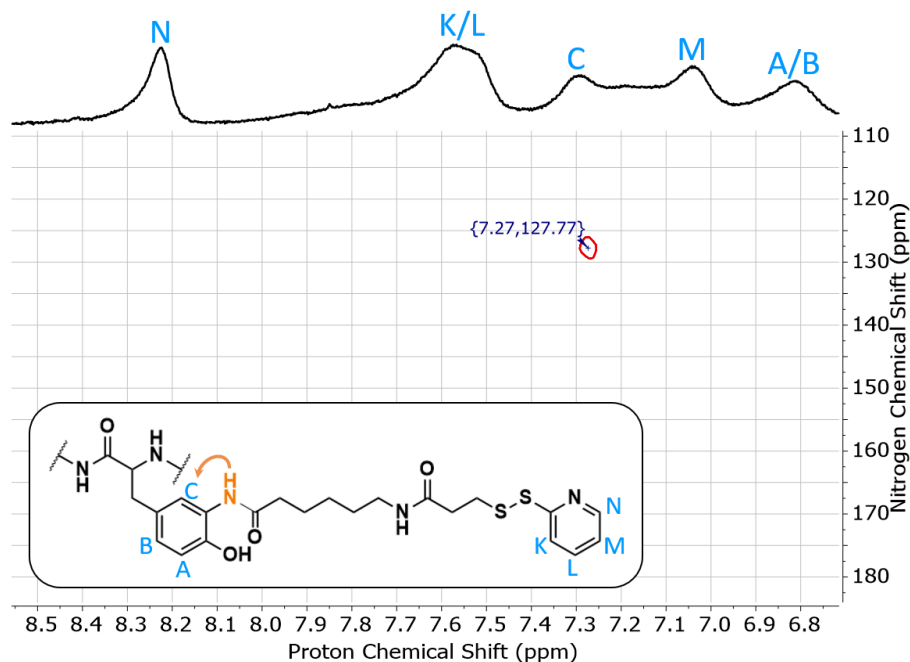


Figure 6. Aromatic region of the ^1H - ^{15}N HMBC of SPDP-modified silk.

3.3 Reduction of SPDP-silk. Once silk was enriched with disulfides from the attachment of sulfo-LC-SPDP, reduction with TCEP·HCl was carried out promptly for the formation of free thiols (Scheme 3). Approximately 3 equivalents (relative to the number of tyrosine residues) of TCEP·HCl was dissolved in 1.5 mL ~1% SPDP-silk in PBS pH 7.2 and allowed to react at room temperature for 10-15 min. By the end of reaction, the solution appeared cloudy perhaps due to the cleavage of the insoluble byproduct, pyridine-2-thione, or from the gelation of silk as a result of intermolecular disulfide formation. For purification, dialysis and size exclusion columns were insufficient to remove excess TCEP and small molecules, therefore centrifugation with a spin concentrator was employed for the purification and concentration of the reaction.

Scheme 3. Reduction of SPDP-silk with TCEP-HCl for the synthesis of thiol-silk.



When the disulfide of SPDP-silk is cleaved, an absence of pyridine proton peaks is noticeable in the proton NMR of thiol-silk and peaks belonging to the cleaved byproduct, pyridine-2-thione, can be observed (Figure 7). Four resonances at 7.9, 7.7, 7.6, and 7.1 are assigned to the four protons on pyridine-2-thione. In the NMR spectrum of purified thiol-silk (Figure 8), only two broad peaks are observed belonging to the remaining tyrosine protons of thiol-silk. Proton C and the aromatic phenyl alanine proton remain at the same chemical shift (7.3 ppm) they were assigned in the NMR of SPDP-silk. The peak assigned to protons A and B of thiol-silk appear to shift slightly downfield at 6.9 ppm compared to their resonance in SPDP-silk (Figure 8B). And most notably, peaks belonging to the pyridine protons N, M, K/L are lacking signifying successful cleavage of the pyridine ring to produce a free thiol moiety.

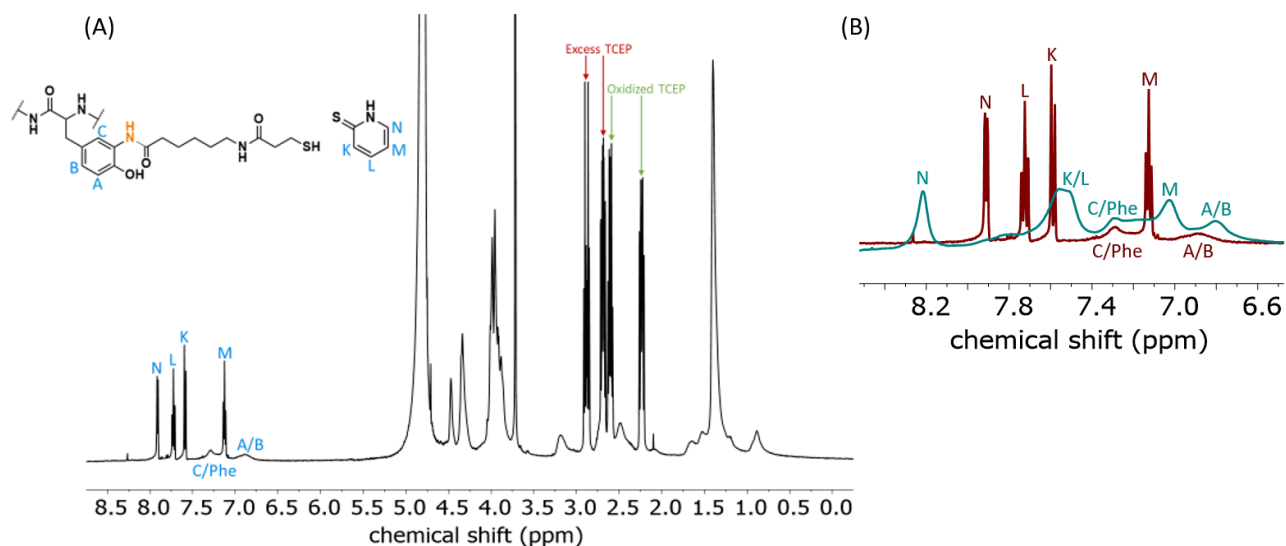


Figure 7. (A) ^1H NMR of thiol-silk containing the cleaved byproduct pyridine-2-thione. (B) Spectra overlay of the aromatic regions of the cleaved byproduct (burgundy) and SPDP-silk (teal).

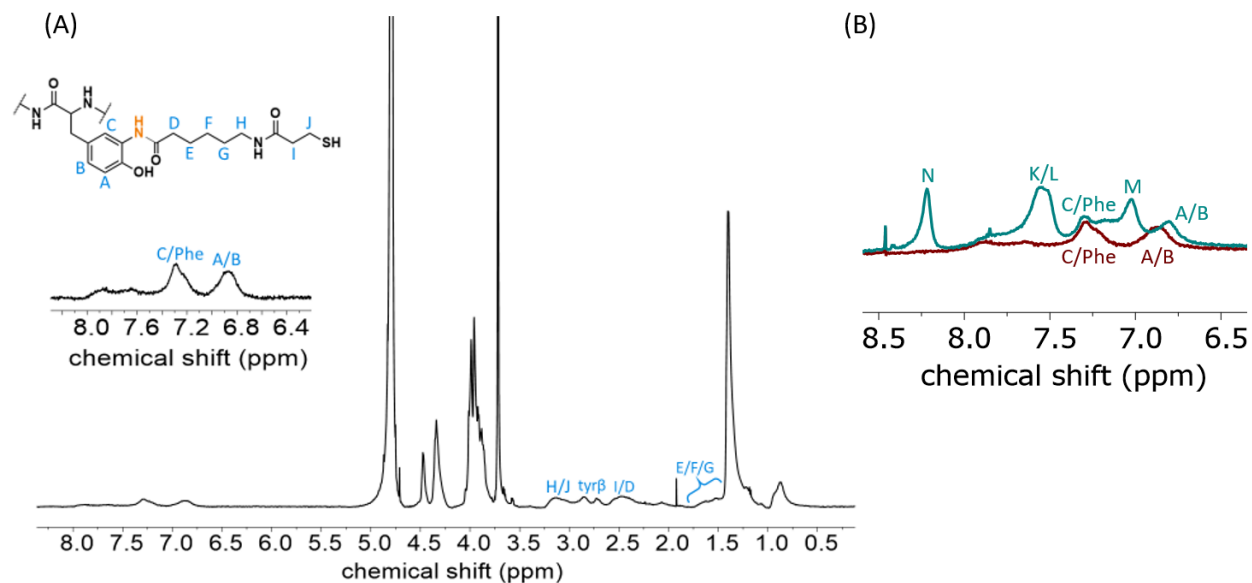


Figure 8. (A) ^1H NMR of thiol-silk with expansion of the aromatic region. (B) Spectra overlay of the aromatic regions of SPDP-silk (teal) and thiol-silk (burgundy).

Pyridine-2-thione (P2T) produces an absorbance at 343 nm, therefore UV-VIS was utilized as another characterization method for the formation of thiol-silk from cleavage of the pyridine ring. SPDP-silk was diluted in 1 mL of PBS pH 7.2 and absorbance was measured. A solution of

TCEP·HCl was added to the same solution and after 10-15 min, absorbance was recorded of the reduced sample. Unmodified tyrosine has an absorbance of 273 nm, and when modified with sulfo-LC-SPDP, the tyrosine peak shifts to 285 nm (Figure 9). After TCEP reduction, the tyrosine peak shifts down to 266 nm and a new peak corresponding to the cleaved disulfide product, P2T, appears at 343 nm. The P2T assay described has been used for the determination of the level of SPDP-modification for proteins, but because the exact concentration of SPDP-silk is unknown, the assay could not be used to confidently quantify the number of tyrosine residues modified with sulfo-LC-SPDP.

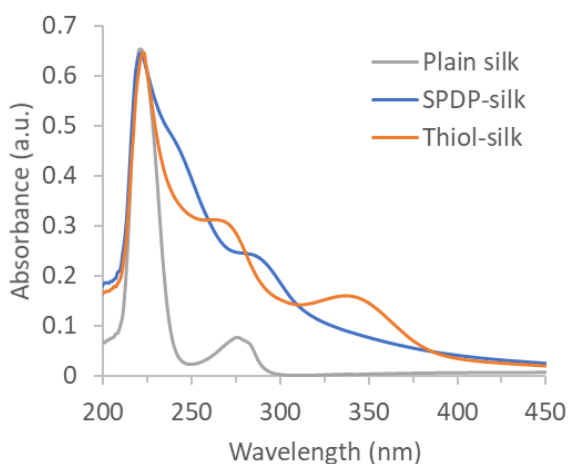
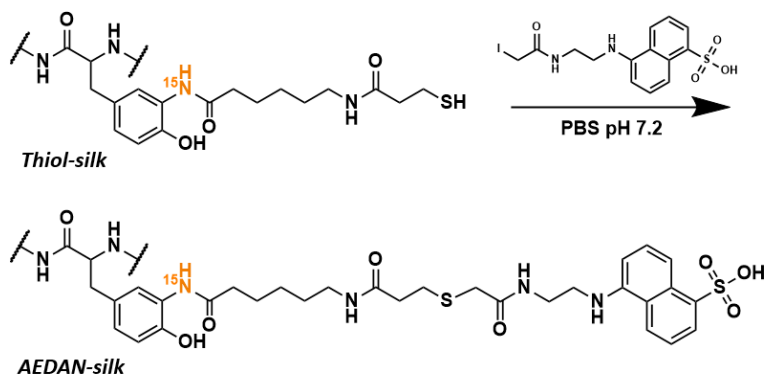


Figure 9. UV-VIS of SPDP-silk and Thiol-silk. Plain silk $\lambda_{\max} = 278$ nm. SPDP-silk $\lambda_{\max} = 285$ nm. Thiol-silk $\lambda_{\max} = 266, 343$ nm.

3.4 Conjugation of IAEDANS to Thiol-Silk. With a reproducible way to incorporate free sulfhydryl groups into silk, the fluorescent molecule 5-(((2-Iodoacetyl)amino)ethyl)amino)naphthalene-1-sulfonic acid, or IAEDANS, was conjugated to thiol-silk to probe the reactivity the of newly installed thiol groups (Scheme 4).

Scheme 4. Conjugation of the fluorescent probe IAEDANS to thiol-silk.



In buffers above pH 4, IAEDANS is highly soluble in water and specific towards thiols to produce a thioether coupled product. Additionally, when excited at 336 nm, IAEDANS has a fluorescent emission at 490 nm, which made it attractive to use to corroborate its conjugation to thiol-silk. Once thiol-silk was produced, 7.5 eq (relative to the number of tyrosine residues) of IAEDANS was dissolved quickly in the silk solution and the reaction was incubated at rt for ~3 h in the dark. After reaction, it was immediately noticed that the IAEDAN modified silk (AEDAN-silk) was more fluorescent than its former silk derivatives, especially upon exposure to UV light, and the AEDAN-silk remained visually fluorescent after being purified with a size exclusion column (Figure 10B). Once purified, fluorescence was collected for AEDAN-silk, SPDP-silk, and amtyr-silk. As shown in Figure 10A, the AEDAN labeled silk displayed a peak emission at 490 nm, a peak absent in the fluorescent spectra of SPDP-silk and amtyr-silk derivatives.

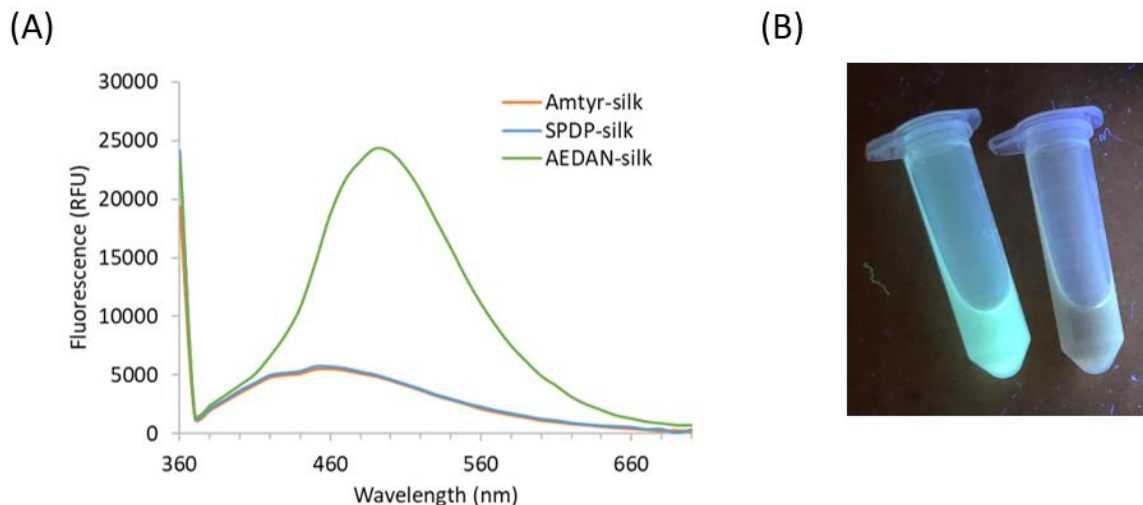


Figure 10. (A) Fluorescence spectra of amtyr-silk, SPDP-silk, and AEDAN-silk $\lambda_{\text{max}} = 490$ (B) Side by side comparison of AEDAN-silk (left) and amtyr-silk (right) under UV light.

Because IAEDANS contains a polycyclic aromatic system, modifications to the thiol-silk could be tracked by evaluating new peaks in the aromatic region of the AEDAN-silk proton NMR (Figure 11). Four new resonances appear in this region, three of which can be assigned to protons of the polycyclic system including a peak at 6.6 ppm corresponding to proton N, a multiplet at 7.3 ppm that can be assigned to protons O, R, S, and a multiplet at 8.0 ppm belonging to protons P and Q. Tyrosine protons A/B appear to shift slightly upfield to 6.9 ppm, while the proton C resonance overlaps with the O/R/S peak. Examining both the proton NMR and fluorescence spectra of AEDAN-silk, the successful conjugation of IAEDANS to the thiol-silk could be confirmed.

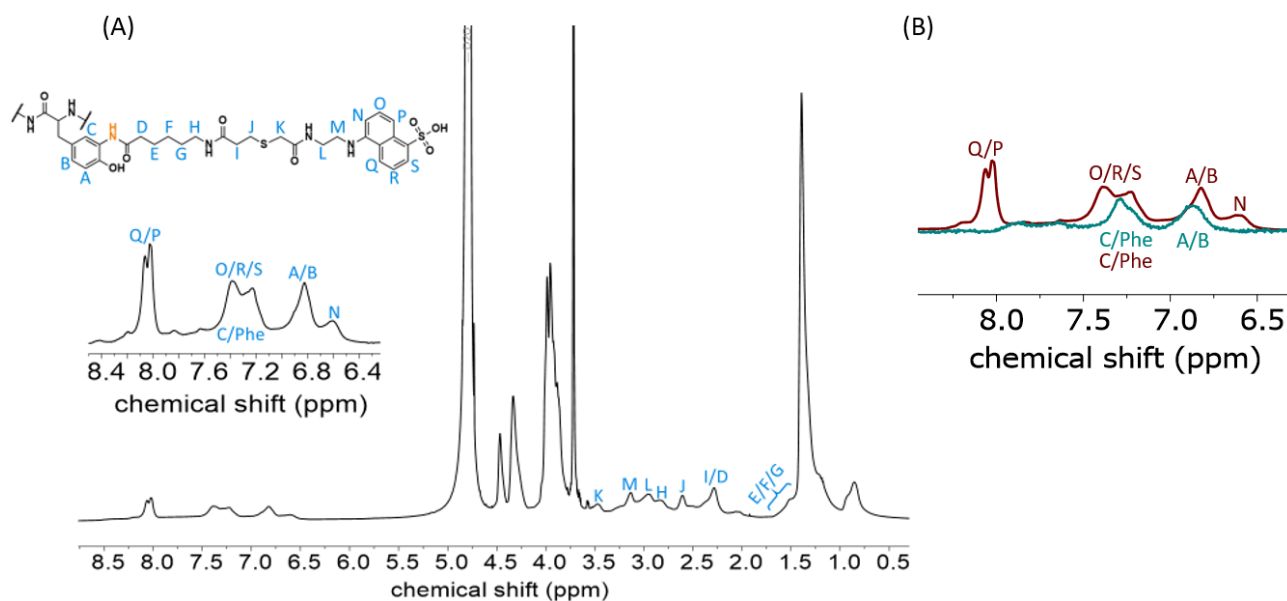


Figure 11. (A) ^1H NMR of AEDAN-silk with expansion of the aromatic region. (B) Spectra overlay of the aromatic regions of thiol-silk (teal) and AEDAN-silk (burgundy).

Since this was the same silk solution that was modified with ^{15}N during the diazonium coupling step, the AEDAN-silk was also characterized using HMBC (Figure 12). Coupling of ^{15}N to proton C remained at the same chemical shift of (7.22, 127.77) ppm compared to the HMBC of SPDP-silk (Figure 6). The conjugation of IAEDANS would understandably not affect the chemical shifts of ^{15}N - ^1H due to the large distance between the site of attachment and the tyrosine ring. The AEDAN-silk HMBC also displayed an additional cross peak at (6.84, 127.77) ppm. Although the peak at 6.84 ppm is shared by both protons A and B of AEDAN-silk, the cross peak presumably arises from the coupling between proton A and ^{15}N due to their closer proximity to one another compared to proton B and ^{15}N .

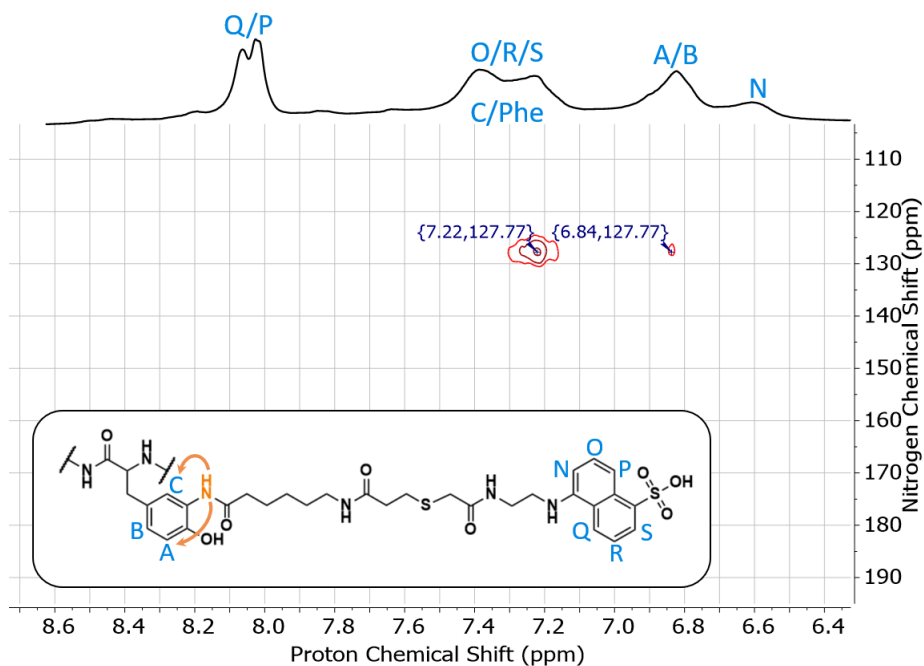
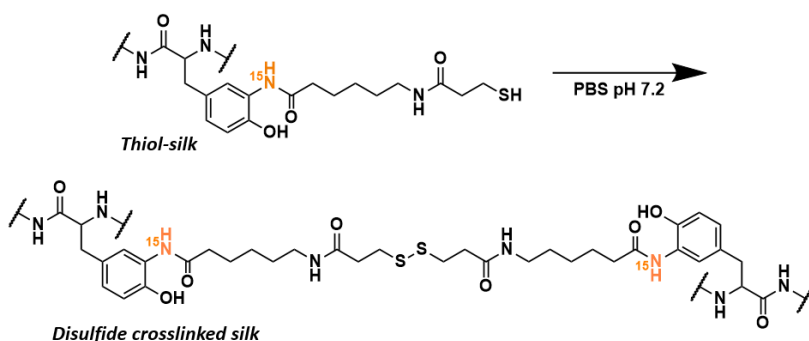


Figure 12. Aromatic region of the ^1H - ^{15}N HMBC of AEDAN-silk.

3.5 *In Situ* Gelation of Thiol-Silk. As mentioned before, one of the attractive properties of thiolated polymers is their ability to undergo *in situ* gelation due to self-crosslinking via disulfide bonds. For this reason, varying concentrations of thiol-silk were investigated for their gelling capabilities (Scheme 5).

Scheme 5. Reduced SPDP-silk can undergo inter- and intramolecular crosslinking through spontaneous disulfide bond formation.



Briefly, thiol-silk solutions were spin concentrated to roughly 10 wt% and diluted with PBS pH 7.2 to give final concentrations of approximately 2.5, 5, and 10 wt% silk. The thiol-silk then sat at rt and gelation was monitored over time. For all concentrations of thiol-silk, the early stage of gelation (the solution-gel transition) was observed within 24 h indicated by a change of clarity of the solution from clear to cloudy. In 3-4 days, the 10 wt% thiol-silk showed complete gelation by tube inversion, as shown in Figure 13A. For 5 wt% thiol-silk solutions, most of the silk appeared gelled by day 12 at rt, but samples contained a small amount of water supernatant (Figure 13B). The 2.5% thiol-silk showed some gelling by inversion, but most of the sample seemed to remain in solution form (Figure 13C). As expected, the polymer network of higher concentrated solutions of silk were able to completely gel in a shorter amount of time. The polymer network of lower concentrated solutions of thiol-silk were unable to retain the large amount of water, and thus could not form a cohesive gel.

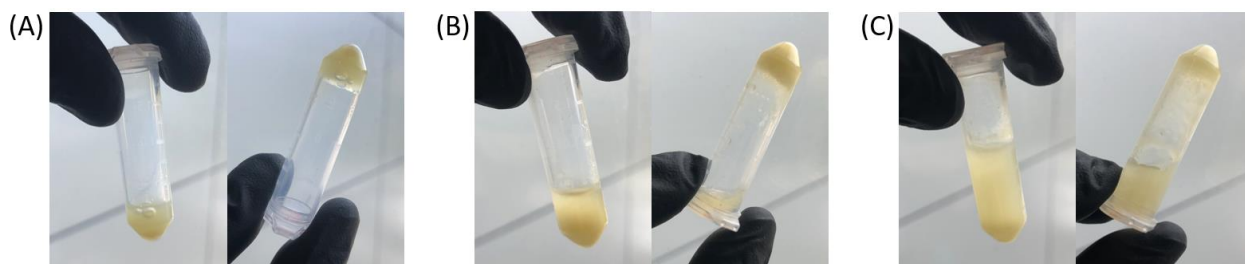


Figure 13. (A) 10 wt % thiol-silk after 4 days at rt (B) 5 wt% thiol-silk after 12 days at rt (C) 2.5 wt% thiol-silk 12 days after rt

Native silk fibroin will naturally increase in β -sheet content over time, forming a hydrogel. The gelation process of silk can be controlled by physical and chemical crosslinks to tune the mechanical properties of the hydrogel.⁴² Although silk fibroin contains only 5.3 mol% of tyrosine, it was envisioned that chemical crosslinks through the tyrosine residues via disulfide bonds would

be enough to rigidify the structure of silk fibroin to form a hydrogel. Therefore, FTIR was employed to determine if the gelation of thiol-modified silk was due to natural β -sheet formation (physical crosslinks) or disulfide bond formation (chemical crosslinks). IR was recorded for dried 10 wt% thiol-silk gel, dried unmodified silk-gel, and lyophilized silk solution for amorphous and crystalline content comparison (Figure 14).

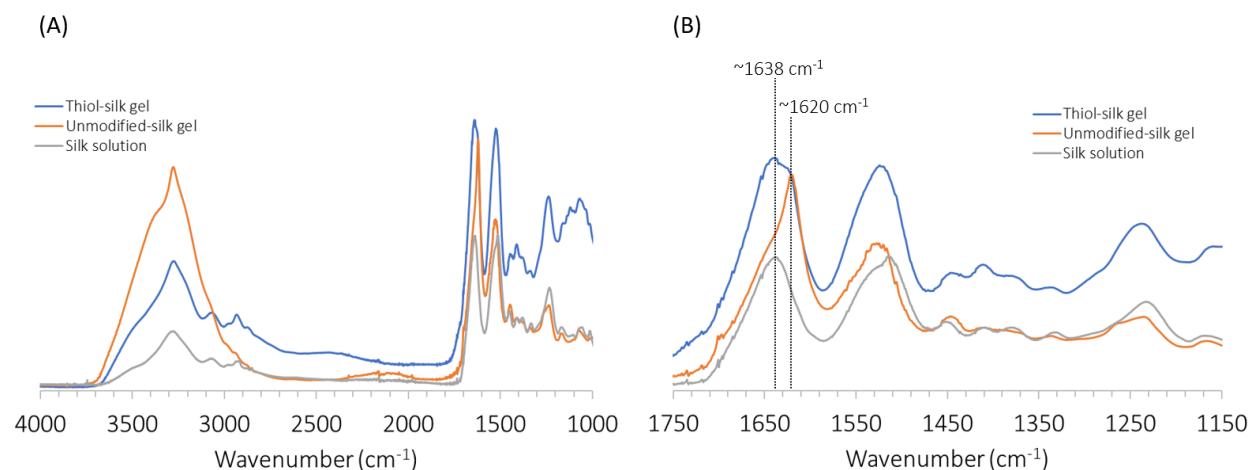


Figure 14. (A) FTIR spectra of thiol-silk gel, unmodified-silk gel, and silk solution (B) Region displaying amide region of silk spectra.

The secondary structure of silk can be determined by examining the amide I (C=O stretch), amide II (N-H bend), and amide III band (C-N bend) of its IR spectrum. For unmodified silk-gel the carbonyl stretch (corresponding to the amides in the silk protein) was observed at 1620 cm⁻¹, consistent with literature values for silk structures that contain a high amount of β -sheet content.⁴³ An absorbance at 1637 cm⁻¹ for the carbonyl of lyophilized silk solution indicated the presence of less ordered, random coil structures. It is very common to see the carbonyl peak shift from higher wavenumbers to lower wavenumbers when silk is physically or chemically crosslinked demonstrating a conformational change of the silk from random coil to more

crystalline arrangements. The carbonyl peak for thiol-silk gel was centered at 1638 cm^{-1} indicating that most of the silk within the gel remained in a random coil state. Therefore, it could be determined that β -sheet formation was not the driving factor for gelation of the thiol-silk. The amide I, II, and III bands of the silk samples are summarized in Table 1.

Table 1. FTIR Vibrational Band Assignments

Silk derivative	C=O stretch (cm^{-1})	N-H bend (cm^{-1})	C-N bend (cm^{-1})
Lyophilized silk solution	1637	1514	1233
Unmodified silk gel	1620	1527	1235
Thiol silk gel	1638	1524	1238

3.6 Rheological Investigation of Thiol-Silk. Rheological measurements are commonly used in the literature to assess the disulfide interaction within thiolated polymers or to other sulfhydryl bearing molecules. Accordingly, apparent viscosity for thiol-silk solutions at varying concentrations were recorded. Thiol-silk solutions were prepared as mentioned above and rheometer measurements were employed after the thiol-silk displayed no more physical changes during its gelation at rt. Unmodified silk solutions of the same concentrations were also prepared and were left to sit at rt for the same amount of time and their viscosities also measured for comparison. In a 15 mm parallel plate geometry, the unmodified silk and thiol-silk were subjected to a constant shear rate of 1/s (no relaxation) at rt and their viscosities averaged over 3 min (summarized in Table 2).

Table 2. Apparent viscosity and shear modulus for varying concentrations of unmodified and thiolated silk at rt and 1 s^{-1} constant shear rate.

Silk derivative	Viscosity (Pa·s)	Shear Modulus (Pa)
2.5 wt%		
Thiol-silk	0.19	0.019
Unmodified silk	0.035	0.004
5 wt%		
Thiol-silk	25.8	2.8
Unmodified silk	0.16	0.016
10 wt%		
Thiol-silk	770	192
Unmodified silk	0.27	0.027

Unmodified 2.5, 5, and 10 wt% silk solutions measured viscosities of 0.035, 0.16, and 0.27 Pa·s, respectively. In the same time period that thiol-silk samples were gelling (maximum of 12 days), all concentrations of unmodified silk remained solutions, yielding low water-like viscosities. In contrast, the viscosities of 2.5, 5, and 10 wt% thiol-silk displayed higher viscosities of 0.19, 26, and 770 Pa·s, respectively, and did appear to undergo a sol-gel transition unlike the unmodified silk. As expected, samples containing a higher concentration of silk protein (unmodified and thiolated) displayed higher viscosities than samples of lower concentrations as a result of a higher degree of disulfide interactions in the thiol-silk, and hydrogen bond interactions in the unmodified silk. All thiolated-silk samples exhibited improved viscosity values compared to their un-thiolated analogues of the same concentration due to inter- and intramolecular disulfide crosslinks within thiol-silk that were absent in unmodified silk samples, a phenomenon also observed in other thiolated polymers such as PAA⁴⁴ and chitosan.⁴¹ The dramatic difference in

viscosities of unmodified silk and thiol-silk highlight the strong disulfide interactions within the thiolated silk and demonstrate that chemical disulfide crosslinks between the tyrosine residues are enough induce gelation.

Chapter 4. Conclusions

In conclusion, silk fibroin was decorated with sulfhydryl handles by the installation of the disulfide containing molecule sulfo-LC-SPDP. Diazonium coupling was performed to form azo bonds on the tyrosine residues of silk followed by reduction with sodium dithionite to create nucleophilic amines ortho to the hydroxyl group on tyrosine. Once the silk was enriched with reactive primary amines they could react with the NHS esters of sulfo-LC-SPDP for the formation of amide bonds. Subsequent reduction of the SPDP-modified silk resulted in the cleavage of disulfide bonds that produced a free thiol moiety and the cleaved product pyridine-2-thione which could be detected by UV-VIS. Once thiols were successfully incorporated into silk, the reactivity of the thiol-silk was probed using a thiol-specific fluorescent iodoacetamide, IAEDANS. Fluorescence was used to support thioether bond formation between IAEDANS and thiol-silk. The fluorescent spectrum of AEDAN-modified silk displayed a peak emission at 490 nm that was absent in preceding silk derivatives, demonstrating the successful reactivity of the sulfhydryl groups. The *in situ* gelling ability of the thiol-silk was also investigated. Gelation via disulfide bond formation was confirmed using FTIR. The inter- and intramolecular disulfide bond formation of different concentrations of thiol-modified silk were measured by increases in viscosity. Thiol-modified silk showed improved viscosities compared to unmodified silk of the same concentrations. Although thiol-silk of lower concentrations still measured higher viscosity values than unmodified silk, the lower concentrated thiol-silk (2.5 wt%) was unable form a cohesive gel network and remained mostly solution.

This research demonstrates the first account of the thiolation of silk fibroin that does not involve modification of the lysine residues of silk or EDC/NHS chemistry. The lack of cysteine residues in silk has limited the use of interesting thiol chemistry that can be performed on silk. Therefore, the installation of thiols through an aminotyrosine intermediate on tyrosine is a promising advancement toward thiol-silk based drug delivery systems.

References

- (1) Rockwood, D. N.; Preda, R. C.; Yücel, T.; Wang, X.; Lovett, M. L.; Kaplan, D. L. Materials Fabrication from Bombyx Mori Silk Fibroin. **2013**, *6* (10), 1–43. <https://doi.org/10.1038/nprot.2011.379.Materials>.
- (2) Li, M.; Ogiso, M.; Minoura, N. Enzymatic Degradation Behavior of Porous Silk Fibroin Sheets. *Biomaterials* **2003**, *24* (2), 357–365. [https://doi.org/10.1016/S0142-9612\(02\)00326-5](https://doi.org/10.1016/S0142-9612(02)00326-5).
- (3) Wang, Y.; Rudym, D. D.; Walsh, A.; Abrahamsen, L.; Kim, H. J.; Kim, H. S.; Kirker-Head, C.; Kaplan, D. L. In Vivo Degradation of Three-Dimensional Silk Fibroin Scaffolds. *Biomaterials* **2008**, *29* (24–25), 3415–3428. <https://doi.org/10.1016/j.biomaterials.2008.05.002>.
- (4) Arai, T.; Freddi, G.; Innocenti, R.; Tsukada, M. Biodegradation of Bombyx Mori Silk Fibroin Fibers and Films. *J. Appl. Polym. Sci.* **2004**, *91* (4), 2383–2390. <https://doi.org/10.1002/app.13393>.
- (5) Colomban, P.; Dinh, H. M.; Bunsell, A.; Mauchamp, B. Origin of the Variability of the Mechanical Properties of Silk Fibres: 1 - The Relationship between Disorder, Hydration and Stress/Strain Behaviour. *J. Raman Spectrosc.* **2012**, *43* (3), 425–432. <https://doi.org/10.1002/jrs.3044>.
- (6) Zhou, C. Z.; Confalonieri, F.; Jacquet, M.; Perasso, R.; Li, Z. G.; Janin, J. Silk Fibroin: Structural Implications of a Remarkable Amino Acid Sequence. *Proteins Struct. Funct. Genet.* **2001**, *44* (2), 119–122. <https://doi.org/10.1002/prot.1078>.
- (7) Jin, H.-J.; Fridrikh, S. V.; Rutledge, G. C.; Kaplan, D. L. Electrospinning Bombyx Mori Silk with Poly(Ethylene Oxide). *Biomacromolecules* **2002**, *3* (6), 1233–1239. <https://doi.org/10.1021/bm025581u>.
- (8) Gangrade, A.; Mandal, B. B. Injectable Carbon Nanotube Impregnated Silk Based Multifunctional Hydrogel for Localized Targeted and On-Demand Anticancer Drug Delivery. *ACS Biomater. Sci. Eng.* **2019**, *5* (5), 2365–2381. <https://doi.org/10.1021/acsbomaterials.9b00416>.
- (9) Numata, K.; Katashima, T.; Sakai, T. State of Water, Molecular Structure, and Cytotoxicity of Silk Hydrogels. *Biomacromolecules* **2011**, *12* (6), 2137–2144. <https://doi.org/10.1021/bm200221u>.
- (10) Kawahara, Y.; Furukawa, K.; Yamamoto, T. Self-Expansion Behavior of Silk Fibroin Film. *Macromol. Mater. Eng.* **2006**, *291* (5), 458–462. <https://doi.org/10.1002/mame.200500350>.
- (11) Cho, Y. J.; Lee, C. H.; Kim, D. W.; Yoo, K. Y.; Eum, W. S.; Shin, M. J.; Jo, H. S.; Park, J.; Han,

- K. H.; Lee, K. W.; et al. Effects of Silk Solution against Laminectomy-Induced Dural Adhesion Formation and Inflammation in a Rat Model. *J. Neurosurg. Spine* **2018**, *29* (5), 599–607. <https://doi.org/10.3171/2018.4.SPINE171164>.
- (12) Severt, S. Y.; Maxwell, S. L.; Bontrager, J. S.; Leger, J. M.; Murphy, A. R. Mimicking Muscle Fiber Structure and Function through Electromechanical Actuation of Electrospun Silk Fiber Bundles. *J. Mater. Chem. B* **2017**, *5* (40), 8105–8114. <https://doi.org/10.1039/c7tb01904a>.
- (13) Sahoo, S.; Lok Toh, S.; Hong Goh, J. C. PLGA Nanofiber-Coated Silk Microfibrous Scaffold for Connective Tissue Engineering. *J. Biomed. Mater. Res. - Part B Appl. Biomater.* **2010**, *95* (1), 19–28. <https://doi.org/10.1002/jbm.b.31678>.
- (14) Johnson, W.; Bergfeld, W. F.; Belsito, D. V.; Hill, R. A.; Klaassen, C. D.; Liebler, D. C.; Marks, J. G.; Shank, R. C.; Slaga, T. J.; Snyder, P. W.; et al. Safety Assessment of Silk Protein Ingredients as Used in Cosmetics. *Int. J. Toxicol.* **2020**, *39* (3_suppl), 127S-144S. <https://doi.org/10.1177/1091581820966953>.
- (15) Zhang, W.; Chen, L.; Chen, J.; Wang, L.; Gui, X.; Ran, J.; Xu, G.; Zhao, H.; Zeng, M.; Ji, J.; et al. Silk Fibroin Biomaterial Shows Safe and Effective Wound Healing in Animal Models and a Randomized Controlled Clinical Trial. *Adv. Healthc. Mater.* **2017**, *6* (10), 1–16. <https://doi.org/10.1002/adhm.201700121>.
- (16) Duff Putu, Jean Shoveller., Julio Montaner., Cindy Feng., Rachel Nicoletti., Kate Shannon ., G. O. Synthesis and Characterization of Silk Fibroin Microparticles for Intra-Articular Drug Delivery. *Physiol. Behav.* **2016**, *176* (1), 139–148. <https://doi.org/10.1016/j.ijpharm.2015.02.059>.Synthesis.
- (17) Zhang, X.; Liang, J.; Chen, Z.; Donley, C.; Liu, Y.; Cheng, G. Chemical Modification of Bombyx Mori Silk Fibers with Vinyl Groups for Thiol-Ene Click Chemistry. *BMC Chem.* **2019**, *13* (1), 114. <https://doi.org/10.1186/s13065-019-0630-7>.
- (18) Wang, X.; Kaplan, D. L. Functionalization of Silk Fibroin with NeutrAvidin and Biotin. *Macromol. Biosci.* **2011**, *11* (1), 100–110. <https://doi.org/10.1002/mabi.201000173>.
- (19) Murphy, A. R.; John, P. S.; Kaplan, D. L. Modification of Silk Fibroin Using Diazonium Coupling Chemistry and the Effects on HMSC Proliferation and Differentiation. *Biomaterials* **2008**, *29* (19), 2829–2838. <https://doi.org/10.1016/j.biomaterials.2008.03.039>.
- (20) Jiang, X.; Chen, Q.; Lin, S.; Shen, J. Surface Modification of Silk Fibroin Films with Zwitterionic Phosphobetaine to Improve the Hemocompatibility. *J. Wuhan Univ. Technol. Mater. Sci. Ed.* **2010**, *25* (6), 969–974. <https://doi.org/10.1007/s11595-010-0131-y>.
- (21) Hermanson, G. T. Zero-Length Crosslinkers. In *Bioconjugate Techniques*; 2013; pp 259–262. <https://doi.org/10.1016/b978-0-12-382239-0.00004-2>.

- (22) Wang, T.; Pfisterer, A.; Kuan, S. L.; Wu, Y.; Dumele, O.; Lamla, M.; Müllen, K.; Weil, T. Cross-Conjugation of DNA, Proteins and Peptides via a PH Switch. *Chem. Sci.* **2013**, *4* (4), 1889–1894. <https://doi.org/10.1039/c3sc22015j>.
- (23) Schnichels, S.; Schneider, N.; Hohenadl, C.; Hurst, J.; Schatz, A.; Januschowski, K.; Spitzer, M. S. Efficacy of Two Different Thiol-Modified Crosslinked Hyaluronate Formulations as Vitreous Replacement Compared to Silicone Oil in a Model of Retinal Detachment. *PLoS One* **2017**, *12* (3). <https://doi.org/10.1371/journal.pone.0172895>.
- (24) Yang, G.; Prestwich, G. D.; Mann, B. K. Thiolated Carboxymethyl-Hyaluronic-Acid-Based Biomaterials Enhance Wound Healing in Rats, Dogs, and Horses. *ISRN Vet. Sci.* **2011**, *2011*, 1–7. <https://doi.org/10.5402/2011/851593>.
- (25) Das, S.; Dhar, B. B. Green Synthesis of Noble Metal Nanoparticles Using Cysteine-Modified Silk Fibroin: Catalysis and Antibacterial Activity †. *R. Soc. Chem.* **2014**. <https://doi.org/10.1039/c4ra06179a>.
- (26) Zhang, X.; Bao, H.; Donley, C.; Liang, J.; Yang, S.; Xu, S. Thiolation and Characterization of Regenerated Bombyx Mori Silk Fibroin Films with Reduced Glutathione. *BMC Chem.* **2019**, *13* (1), 1–9. <https://doi.org/10.1186/s13065-019-0583-x>.
- (27) Laomeephol, C.; Ferreira, H.; Yodmuang, S.; Reis, R. L.; Damrongsakkul, S.; Neves, N. M. Exploring the Gelation Mechanisms and Cytocompatibility of Gold (III)-Mediated Regenerated and Thiolated Silk Fibroin Hydrogels. *Biomolecules* **2020**, *10* (3), 1–14. <https://doi.org/10.3390/biom10030466>.
- (28) Ryu, S.; Kim, H. H.; Park, Y. H.; Lin, C. C.; Um, I. C.; Ki, C. S. Dual Mode Gelation Behavior of Silk Fibroin Microgel Embedded Poly(Ethylene Glycol) Hydrogels. *J. Mater. Chem. B* **2016**, *4* (26), 4574–4584. <https://doi.org/10.1039/c6tb00896h>.
- (29) Smart, J. D. The Basics and Underlying Mechanisms of Mucoadhesion. *Adv. Drug Deliv. Rev.* **2005**, *57* (11), 1556–1568. <https://doi.org/10.1016/j.addr.2005.07.001>.
- (30) Birchenough, G. M. H.; Johansson, M. E. V.; Gustafsson, J. K.; Bergström, J. H.; Hansson, G. C. New Developments in Goblet Cell Mucus Secretion and Function. *Mucosal Immunol.* **2015**, *8* (4), 712–719. <https://doi.org/10.1038/mi.2015.32>.
- (31) Lehr, C. M.; Bouwstra, J. A.; Schacht, E. H.; Junginger, H. E. In Vitro Evaluation of Mucoadhesive Properties of Chitosan and Some Other Natural Polymers. *Int. J. Pharm.* **1992**, *78* (1–3), 43–48. [https://doi.org/10.1016/0378-5173\(92\)90353-4](https://doi.org/10.1016/0378-5173(92)90353-4).
- (32) Park, H.; Robinson, J. R. Mechanisms of Mucoadhesion of Poly(Acrylic Acid) Hydrogels. *Pharmaceutical Research: An Official Journal of the American Association of Pharmaceutical Scientists.* 1987, pp 457–464. <https://doi.org/10.1023/A:1016467219657>.
- (33) Malmsten, M.; Ljusegren, I.; Carlstedt, I. Ellipsometry Studies of the Mucoadhesion of

- Cellulose Derivatives. *Colloids Surfaces B Biointerfaces* **1994**, *2* (5), 463–470. [https://doi.org/10.1016/0927-7765\(94\)80054-5](https://doi.org/10.1016/0927-7765(94)80054-5).
- (34) Leitner, V. M.; Walker, G. F.; Bernkop-Schnürch, A. Thiolated Polymers: Evidence for the Formation of Disulphide Bonds with Mucus Glycoproteins. *Eur. J. Pharm. Biopharm.* **2003**, *56* (2), 207–214. [https://doi.org/10.1016/S0939-6411\(03\)00061-4](https://doi.org/10.1016/S0939-6411(03)00061-4).
- (35) Puri, V.; Sharma, A.; Kumar, P.; Singh, I. Thiolation of Biopolymers for Developing Drug Delivery Systems with Enhanced Mechanical and Mucoadhesive Properties: A Review. *Polymers (Basel)*. **2020**, *12* (8). <https://doi.org/10.3390/polym12081803>.
- (36) Makhlof, A.; Werle, M.; Tozuka, Y.; Takeuchi, H. Nanoparticles of Glycol Chitosan and Its Thiolated Derivative Significantly Improved the Pulmonary Delivery of Calcitonin. *Int. J. Pharm.* **2010**, *397* (1–2), 92–95. <https://doi.org/10.1016/j.ijpharm.2010.07.001>.
- (37) Ways, T. M. M.; Lau, W. M.; Khutoryanskiy, V. V. Chitosan and Its Derivatives for Application in Mucoadhesive Drug Delivery Systems. *Polymers (Basel)*. **2018**, *10* (3). <https://doi.org/10.3390/polym10030267>.
- (38) Cevher, E.; Taha, M. A. M.; Orlu, M.; Araman, A. Evaluation of Mechanical and Mucoadhesive Properties of Clomiphene Citrate Gel Formulations Containing Carbomers and Their Thiolated Derivatives. *Drug Deliv.* **2008**, *15* (1), 57–67. <https://doi.org/10.1080/10717540701829234>.
- (39) Duggan, S.; O'Donovan, O.; Owens, E.; Duggan, E.; Hughes, H.; Cummins, W. Comparison of the Mucoadhesive Properties of Thiolated Polyacrylic Acid to Thiolated Polyallylamine. *Int. J. Pharm.* **2016**, *498* (1–2), 245–253. <https://doi.org/10.1016/j.ijpharm.2015.12.036>.
- (40) Naz, K.; Shahnaz, G.; Ahmed, N.; Qureshi, N. A.; Sarwar, H. S.; Imran, M.; Khan, G. M. Formulation and In Vitro Characterization of Thiolated Buccoadhesive Film of Fluconazole. *AAPS PharmSciTech* **2017**, *18* (4), 1043–1055. <https://doi.org/10.1208/s12249-016-0607-y>.
- (41) Sakloetsakun, D.; Hombach, J. M. R.; Bernkop-Schnürch, A. In Situ Gelling Properties of Chitosan-Thioglycolic Acid Conjugate in the Presence of Oxidizing Agents. *Biomaterials* **2009**, *30* (31), 6151–6157. <https://doi.org/10.1016/j.biomaterials.2009.07.060>.
- (42) Farokhi, M. Crosslinking Strategies for Silk Fibroin Hydrogels: Promising Biomedical Materials. *Biomed. Mater.* **2021**, *16*.
- (43) Chen, X.; Shao, Z.; P. Knight, D.; Vollrath, F. Conformation Transition Kinetics of Bombyx Mori Silk Protein. *Proteins Struct. Funct. Bioinformatics* **2007**, *68* (1), 223–231. <https://doi.org/10.1002/prot.21414>.
- (44) Marschütz, M. K.; Bernkop-Schnürch, A. Thiolated Polymers: Self-Crosslinking Properties of Thiolated 450 KDa Poly(Acrylic Acid) and Their Influence on Mucoadhesion. *Eur. J. Pharm. Sci.* **2002**, *15* (4), 387–394. [https://doi.org/10.1016/S0928-0987\(02\)00025-8](https://doi.org/10.1016/S0928-0987(02)00025-8).

- (45) Liu, J.; Yang, B.; Li, M.; Li, J.; Wan, Y. Enhanced Dual Network Hydrogels Consisting of Thiolated Chitosan and Silk Fibroin for Cartilage Tissue Engineering. *Carbohydr. Polym.* **2020**, 227 (August 2019), 115335. <https://doi.org/10.1016/j.carbpol.2019.115335>.